Aerospace Science and Technology 147 (2024) 109017

Contents lists available at ScienceDirect

Aerospace Science and Technology

journal homepage: www.elsevier.com/locate/aescte

Aerodynamic interaction between tandem propellers in eVTOL transition flight configurations

Alex Zanotti *, Alessandro Velo, Chiara Pepe, Alberto Savino, Donato Grassi, Luca Riccobene

Politecnico di Milano, Dipartimento di Scienze e Tecnologie Aerospaziali, via La Masa 34, 20156, Milan, Italy

ARTICLE INFO

Communicated by Damiano Casalino

Keywords:
Aerodynamics
Wind tunnel
Particle image velocimetry
Vortex particle method
eVTOL

ABSTRACT

The present study investigates the aerodynamic interactions in a tandem propellers configuration typical of a tilt-wing eVTOL aircraft during the transition manoeuvre. Particular focus is on how the relative position and the propeller's tilting angle influence the aerodynamic performance. A systematic series of wind tunnel tests, including thrust and torque measurements with Particle Image Velocimetry (PIV) surveys, were performed on two co-rotating propellers models with fixed axial distance while the propellers tilting angle and the lateral separation distance were changed. The comprehensive wind tunnel campaign explored all the phases of the transition from take-off to cruise, thus highlighting possible detrimental effects on the multi-rotor system due to aerodynamic interactional mechanisms occurring due to front propeller impingement on rear propeller disks. To achieve detailed insights into the physical comprehension of the complex interactional effects produced on the rear propeller disk, the activity was completed by a numerical investigation performed through the mid-fidelity solver DUST, based on Vortex Particle Method for the wake modelling. From the perspective of a preliminary design phase of eVTOL concepts, this work showed that particular attention must be paid to the transition flight regime since both the tilting angle of attack of propellers and the free-stream velocity heavily affects the propulsive system behaviour. As a general outcome, higher vertical distances between propellers guarantee to reduce the performance losses on the rear propeller despite the presence of mutual interference phenomena.

1. Introduction

Increasing demand for reduced traffic congestion, combined with the need for sustainable solutions to be adopted, pushes towards the development of new concept vehicles, classified as eVTOLs (Electric Vertical Take Off and Landing). In the framework of the growing market of Urban Air Mobility (UAM), one of the main challenges is represented by the limited spaces available for building new large infrastructures. For this reason, the introduction of VTOLs is an attractive solution to ensure the possibility of vertical take-off and landing, together with the comfort and performance typical of fixed-wing aircraft in cruise condition. Another important element to consider correlated to the operative and performance requirements is the necessity to introduce such vehicles in an urban reality without compromising environmental integrity. The negative effects of traffic congestion in the urban environment highlight the compelling necessity of a new type of public transportation service able to combine a reduction in the time spent travelling and the amount of urban pollution. The UAM reality automatically stands out in the evolution of urban mobility as the most innovative solution, since it exploits the third dimension of the aerial space.

In this current framework, eVTOLs represent the most viable solution to combine at the same time the improvement in urban mobility and the regulation of emissions with respect to traditional vehicles like helicopters. The most peculiar common feature of various eVTOL configurations is the implementation of a distributed electric propulsion (DEP) system, composed of multiple propellers distributed on different lifting surfaces. Regarding this innovative system, Silva and Johnson [1] presented some conceptual designs of multi-propellers architectures that meet the main requirements imposed by UAM market. Their work highlights various benefits deriving from such systems, which can be grouped into two main aspects. First, the achievement of redundancy ensures larger safety margins in case of one propeller inoperative and higher possibilities to better control the aircraft. Second, rotors are smaller and simpler with respect to traditional helicopters, thus enabling easier control in terms of propellers RPM. Additionally, as they are all designed in the same way, they lead to a less complex and time

* Corresponding author.
E-mail address: Alex.Zanotti@polimi.it (A. Zanotti).

https://doi.org/10.1016/j.ast.2024.109017
Received 30 January 2024; Received in revised form 14 February 2024; Accepted 24 February 2024
Available online 1 March 2024

Notation

CFD	Computational Fluid Dynamics		
C_P	power coefficient, $= P/(\rho n^3 D^5)$		
C_Q	power coefficient $= Q/(\rho n^2 D^5)$		
C_T	thrust coefficient $= T/(\rho n^2 D^4)$		
D	propeller diameter	m	
eVTOL	electrical Vertical Take Off and Landing aircraft		
J	advance ratio $= V_\infty/(nD)$		
D_x	longitudinal distance between the propeller disks		
D_y	lateral distance between the propeller axis		
M_t	tip Mach number		
n	rotational speed	rad/s	
P	propeller power	W	
Q	propeller torque	Nm	
r	propeller blade radial coordinate	m	
R	propeller blade radius	m	
T	propeller thrust	N	
u	sectional propellers blades axial velocity component	m/s	
w	sectional propellers blades tangential velocity component	m/s	
UAM	Urban Air Mobility		
VPM	Vortex Particle Method		
V	in-plane velocity magnitude	m/s	
V_∞	wind tunnel freestream velocity	m/s	
$X-Y-Z$	reference system		
α	sectional propellers blades angle of attack	deg	
α_P	propellers tilting angle of attack	deg	
ψ	blade azimuthal angle	deg	
ρ	air density	kg/m^3	
θ	blade pitch angle at 75% of the rotor radius	deg	

Subscripts

rp	rear propeller
sp	single propeller

demanding design phase, which translates into important economic benefits and easier logistic management.

Nevertheless, a demanding challenge is represented by the achievement of a complete technological maturity of eVTOLs, which must go through several aspects. Firstly, the necessity of a significant reduction of environmental impact through the adoption of electric power brings the need for powerful and long-lasting batteries with a high rate of charging, such as to allow high-frequency operations. Additionally, as stressed by the general reviews by Silva [1] and Kim [2] rotor-rotor aerodynamic interaction represents one of the main challenges associated with eVTOLs development. Indeed, the arise of propellers aerodynamic interaction phenomena, both mutual and with lifting surfaces, may cause detrimental effects on the performance and control capability of the vehicle. Thus, an increasing interest in propeller/propeller mutual influence can be noted in the literature. In particular, despite the remarkable differences occurring between helicopters, UAVs, and eVTOLs, worthwhile and relevant information can be collected from previous studies to give a general overview of possible interactional phenomena generated by a multi-rotor configuration.

In the field of classical helicopters, the work by Ramasamy [3] provides a first estimation of loss factors in terms of thrust and hovering efficiency through the comparison between a single rotor and different tandem configurations over a wide range of lateral separation distances. For what concerns UAVs applications, Shukla [4] performed an experimental analysis of the aerodynamic interaction between two small propellers positioned in a side-by-side configuration to simulate the in-plane multi-rotor distribution typical of UAVs. The inter-rotor wake behaviour is investigated for different values of the axial distance and for two distinct Reynolds numbers, to simulate the operative conditions of UAVs and to evaluate the effects of the rotors separation on performance. Results obtained through the SPIV (Stereo Particle Image Velocimetry) and load measurements highlight a performance drop for decreasing values of the axial offset. The aforementioned studies are fundamental to introduce the effects of the aerodynamic interaction between rotors in close proximity typical of eVTOLs concepts, based on a DEP architecture with multi-propellers configurations.

An analysis of a distributed propulsion system was provided by De Vries [5], whose work was focused on the investigation of the aerodynamic behaviour of three propellers in side-by-side attitude. Authors widely investigated the main sources and causes of efficiency loss of the system, focusing their attention on the effect of adjacent propellers on aerodynamic performance of the middle one, particularly highlighting the important contribution deriving from the angle of attack.

In the work by Stokkermans [6], two different types of propeller-propeller interactions were distinguished, i.e. side by side and one-after-another. All configurations were investigated by means of wind tunnel tests, while a low-order numerical model as blade element theory was exploited for the analysis of the one-after-another case. Authors performed a parametric study of the aerodynamic interaction between side-by-side propellers at different angles of attack, varying both the horizontal distance between rotor axes and the vertical separation between propellers disks. For what concerns the one-after-another configuration the strong dependency of thrust and power coefficients on lateral distance between propellers axes can be explained by the different region of impingement of the front propeller slipstream on the rear rotor. In particular, for high lateral distances and co-rotating propellers, the slipstream produces an increase in the effective angle of attack of the rear propeller blades in the overlapping region, hence partially compensating performance losses. On the contrary, for low lateral distances the rear propeller blades are affected by a reduction of the angle of attack.

Moreover, Zanotti and Algarotti [7] and Piccinini et al. [8] investigated aerodynamic interaction between tandem overlapping propellers in cruise conditions, both using wind tunnel tests and numerical simulations using mid-fidelity solver DUST. Both experimental and numerical findings reveal propellers performance losses that enlarge for decreasing values of lateral distances. In particular, with a certain degree of disks overlap, the slipstream of the front propeller impinges on the rear one and leads to a local increment of advance ratio, which in turn affects rear propeller performance. The complete overlapping configuration turns out to be the most detrimental one, with thrust penalties for the rear propeller up to 30%.

As can be deduced from literature review, most of the works dedicated to the investigation multi-rotor aerodynamic interaction are focused on hover or cruise flight conditions. However, among the most investigated eVTOL architectures, vectored thrust eVTOLs are affected by the transition phase from hover to cruise configuration, hence a thorough analysis of this phase is fundamental for the development of such vehicles. A certain gap in the analysis of this flight condition in present in literature. Indeed, only few works aimed at investigate the transition phase can be found in literature, mainly applied to tiltrotor concept. An experimental investigation by Droandi et al. [9], provided a detailed analysis of the aerodynamic interference between wing and rotor during the first phase of the conversion manoeuvre for a tilt-wing configuration. The aim of their work was to evaluate the interference effects between the partially tilted wing and the slipstream of the rotor through the analysis of load distribution as function of advance ratio, tilting angle of the nacelle and of the tilted portion of the wing. Moreover, considering numerical studies, Sheng et al. [10] performed a numerical simulation of the Bell Boeing QuadTilt Rotor concept to investigate

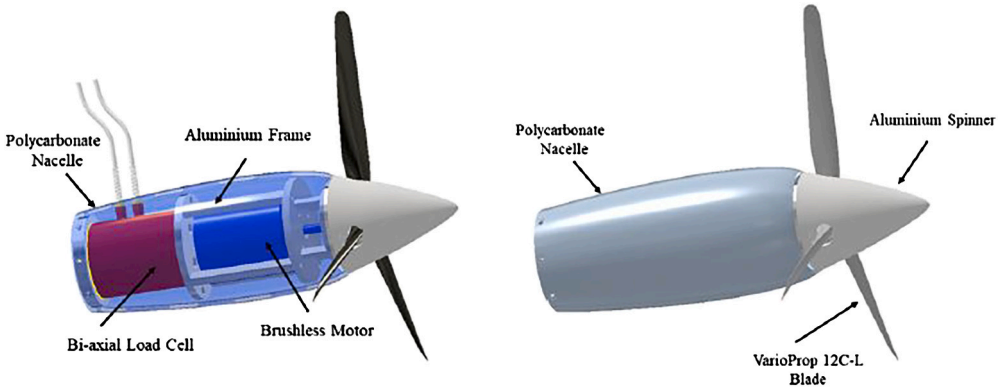

Fig. 1. Render of the propeller model, from [14].

two different configurations, i.e. cruise flight and transition phase with a nacelle tilt angle of 75°, to evaluate the aerodynamic interference between front rotors and wings. Despite these projects, a substantial lack in previous works is found for what concerns the aerodynamic interaction between propellers in the transition manoeuvre with only exception represented by results coming from the experimental activity by Stokkermans et al. [6] previously outlined, investigating propellers configurations with a certain angle of attack.

Transition phase of tilt-wing eVTOLs inherits the critical aspects occurring during the development of first tiltrotor concepts, with the added complexity introduced by a multi-propeller configuration and by the presence of multiple tilting lifting surfaces. Indeed, in a traditional tiltrotor configuration, a single lifting surface is used and the relative distance between the two tilting rotors is quite large. Thus, the mutual interference between the two rotors can be neglected without introducing significant errors. Instead, a tilt-wing eVTOL configuration as the Airbus Vahana [11] introduces additional elements to be taken into account due to the presence of two interacting lifting surfaces with distributed propulsive systems that simultaneously tilt during the transition manoeuvre. Such a configuration extends the issue of interaction to the rotor-rotor interference as the slipstreams of propellers placed on the front tilt-wing may invest the propellers positioned on the rear lifting surface and affect their performance.

The aim of the present work is therefore to improve knowledge about tandem propellers aerodynamic interactions by filling the lack related to the study of interacting flow mechanisms occurring in a multi-rotor configurations from hover to airplane mode flight conditions. Indeed, a systematic series of wind tunnel tests were performed on two propeller models in tandem configuration by changing their lateral separation distance at fixed axial distance. Moreover, the propellers tilting angle with the incoming flow was progressively changed to reproduce steady-state points of the complete transition manoeuvre from helicopter to aircraft mode, while the free-stream velocity was accordingly varied. Measurements spanning configurations with tilting angle of attack for a tandem propeller system represent the main novelty of the present work and are aimed to fill the outcomes obtained by the previous activity by Zanotti and Algarotti [7] focused on cruise flight conditions. Wind tunnel tests included loads measurements to evaluate, particularly, the effects on rear propeller performance provided by aerodynamic interaction of front propeller slipstream. Moreover, PIV surveys were performed to accurately evaluate novel insights about the interacting flow field between propellers wakes. In addition to experimental activity, numerical simulations reproducing some selected wind tunnel test configurations were performed using the mid-fidelity aerodynamic solver DUST [12]. The numerical activity was aimed to provide insights useful to enhance the physical comprehension of the interactional mechanisms for such complex flow conditions. Generally, the present activity was aimed to provide a free comprehensive experimental database over a wide set of tandem propellers configurations to be considered as a novel and suitable tool for scientific and industrial communities to validate numerical solvers and to guide the design of eVTOLs architectures.

The paper is organized as follows. Section §2 describes the experimental setup, including propeller model design, measurement techniques, and definition of the test configurations. Section §3 describes the numerical model built in DUST for the simulations of the tandem propeller configurations. Section §4 presents the discussion of the main results obtained by both experiments and simulations for the different transition flight configurations reproduced in the wind tunnel. Conclusions are drawn in Sec. §5.

2. Experimental set up

The experimental activity was performed at the *S. De Ponte* wind tunnel of Politecnico di Milano. The closed-loop wind tunnel has a 1 m × 1.5 m test section and can reach a maximum speed of 55 $m\,s^{-1}$ with a turbulence level lower than 0.1%.

2.1. Propeller models set up

Two propeller models were designed and manufactured for the wind tunnel test campaign. The models were the same used for the test activity described in [13]. Fig. 1 shows the render of the propeller model highlighting the internal layout.

The propeller hub was designed using hobby-grade components. In particular, a three-bladed hub equipped with left-handed VarioProp 12C blades was used, thus resulting in a propeller disk diameter D equal to 300 mm. A 65 mm diameter aluminium spinner was screwed on the propeller hub. An internal aluminium frame was designed to support the propeller driving system and a bi-axial strain gauge load cell. The propeller was driven by a Scorpion brushless motor (5.3 kW continuous power) with shaft connected directly to propeller hub. The motor was powered by an external PWM-controlled electronic speed controller. A custom software developed in Labview was used to keep controlled both propellers at the desired rotational speed. A maximum fluctuation below 1% of the target rotational speed of the propellers was found during the wind tunnel tests. Blade azimuth phases of the two propellers blades were not synchronised as done in [15,16,13] due to hardware limitation of the hobby-grade external speed controller available for the tests. A polycarbonate nacelle with 270 mm length was manufactured using FDM technique and mounted on the internal metallic frame to shield both the motor and the load cell.

Propeller models were positioned within the test chamber using a framework constructed from 30 mm × 30 mm squared section aluminium Bosch© tubes, affording flexibility in configuring their placement inside the chamber. A polystyrene airfoil-shaped leading edge was attached to the front end of the tube to reduce aerodynamic interference. The two propellers were mounted in tandem configuration with

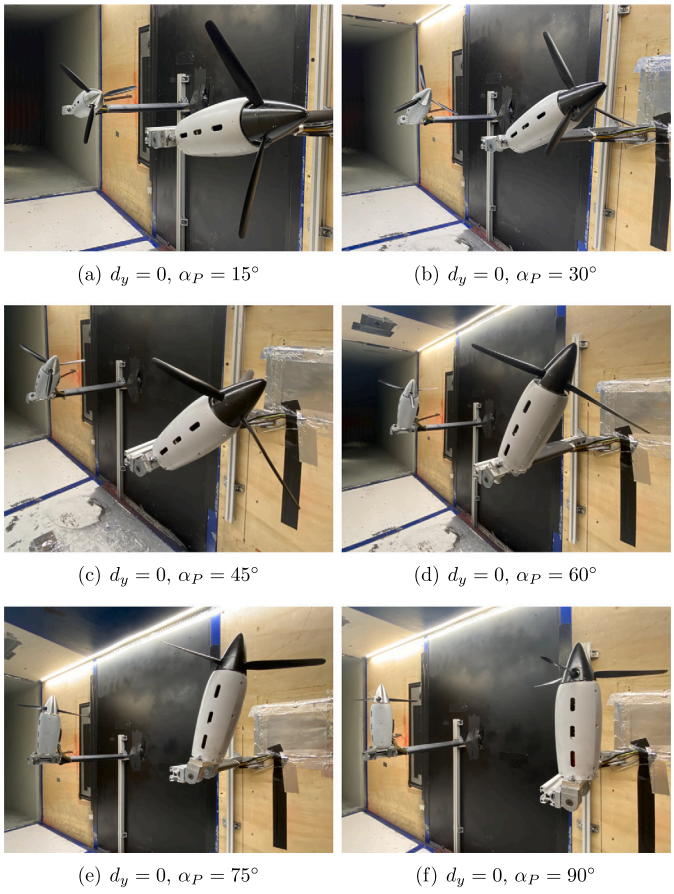

(a) $d_y = 0$, $\alpha_P = 15°$ (b) $d_y = 0$, $\alpha_P = 30°$

(c) $d_y = 0$, $\alpha_P = 45°$ (d) $d_y = 0$, $\alpha_P = 60°$

(e) $d_y = 0$, $\alpha_P = 75°$ (f) $d_y = 0$, $\alpha_P = 90°$

Fig. 2. Wind tunnel setup for the co-axial tandem configurations at the different tilting angles tested α_P.

an axial distance (D_x) between the propellers disk equal to 5 rotor radii, selected to reproduce a Vahana-like architecture. The aluminium strut attached to one of the test section lateral walls, acting as a rail, enabled to manually modify the lateral separation distance between the models. In particular, the front propeller vertical position (D_y) was modified during the experimental campaign, while propellers tilting angle α_P setting was made using a rolling joint by Bosch© attached to the supporting strut. Propellers were tilted along their longitudinal axis lying on mid-span plane of the test chamber. Fig. 2 shows some pictures of the two co-axial propellers in the wind tunnel at the different tilting angles tested, while Fig. 3 shows the tandem propellers at different vertical distances for a single tilting angle.

2.2. Loads measurements set up

A Futek MBA500 strain gauge bi-axial load cell embedded in the internal metallic structure (see Fig. 1) was used to measure propellers thrust and torque. Load cell has a F.S. range of ±50 lbs for thrust and of ±50 lbs-in for torque (non-linearity ±0.25% R.O., non-repeatability ±0.05% R.O.). The load cell signals were acquired by a National Instrument c-DAQ system equipped with a strain/bridge NI 9237 module. Loads signals were sampled at 25 kHz and averaged over 10 seconds of acquisition time. Each test point was measured four times and results averaged. Details about measurements accuracy evaluated by several measurements repetitions with the same set up are reported in [13]. Propellers loads and rotational speed were acquired simultaneously to wind tunnel parameters (i.e. dynamic pressure, air temperature, air relative humidity, atmospheric pressure) by a custom software developed using LabView.

Wind tunnel wall corrections were applied to performance data of single propeller tests. Due to the substantial lack of literature regarding empirical or analytical expressions accounting for blockage effects in tandem propellers configuration in a closed test section, corrections were omitted for the tandem propellers performance data, as done in [6]. This choice was supported considering the almost negligible variations of advance ratio found in the single propeller case. In particular, a solid blockage correction below 1% of advance ratio was found for the worst test condition characterised by $\alpha_P = 90°$. Moreover, wake blockage effect was evaluated as described by Hackett et al. [17]. In this method, propeller is represented as a sink and thrust coefficient is multiplied by $\cos(\alpha_P)$ to consider only the component aligned with the wind tunnel longitudinal direction for the non-zero incidence cases, as also reported by Stokkermans et al. [18].

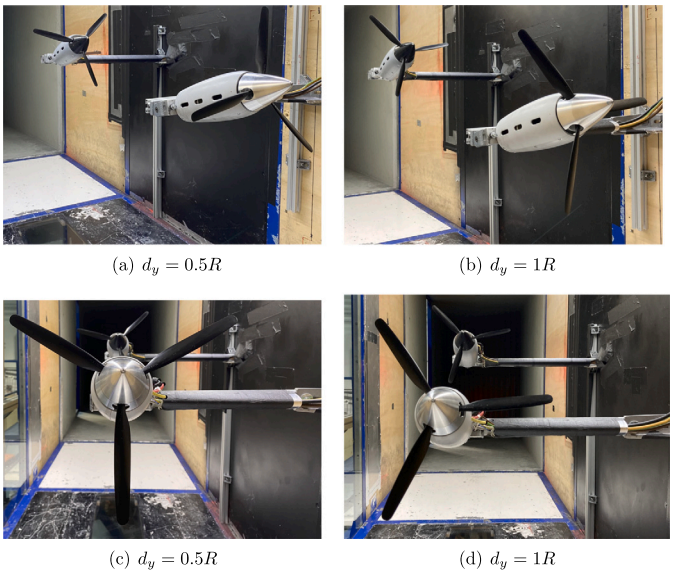

(a) $d_y = 0.5R$ (b) $d_y = 1R$

(c) $d_y = 0.5R$ (d) $d_y = 1R$

Fig. 3. Tandem propellers configurations with different vertical distances D_y at tilting angle of attack $\alpha_P = 15°$, (a-b) lateral view and (c-d) front views.

2.3. PIV set up

Two-components PIV surveys were performed in this wind tunnel campaign. The set up of the instrumentation is shown in Fig. 4. A Quantel Evergreen Nd:Yag double-pulse laser with an output energy of 200 mJ and wavelength of 532 nm was positioned under the plexiglass floor of wind tunnel test section to generate a laser sheet aligned with the longitudinal $X - Y$ mid-span plane by means of a 90° optic mirror. Two double-shutter ILA.PIV.sCMOS cameras with a 16 bit 2560×2160 pixels array were mounted on an external metallic structure around the test section. The cameras were positioned in tandem configuration (Upper and Lower camera in Fig. 4) to enlarge the wake flow region of survey around the rear propeller. This solution enabled to frame an interesting flow area for all the tilting angle of attack tested without changing the cameras position. A particle generator (PIVpart30 by PIVTEC) equipped with Laskin atomizer nozzles was used to fulfil wind tunnel test section with seeding. The seeding particles consisted of small oil droplets with a diameter in the range of 1–2 μm.

Free-run 2C measurements over 200 image pairs were performed for each test configuration considered during the wind tunnel campaign and results were ensemble averaged. Image pairs analysis was performed using PIVview 3C software developed by PIVTEC. Post-processing made use of the multi-grid interrogation method [19] starting from a 128 pixels × 128 pixels to a 16 pixels × 16 pixels interrogation window with effective 50% overlap. This methodology results in a spatial resolution between adjacent measurement points less than 2 mm. As the flow regions shadowed by rear propeller blades and nacelle depended on tilting angle of attack, the dimensions of the output areas of investigation were different as will be shown in the results discus-

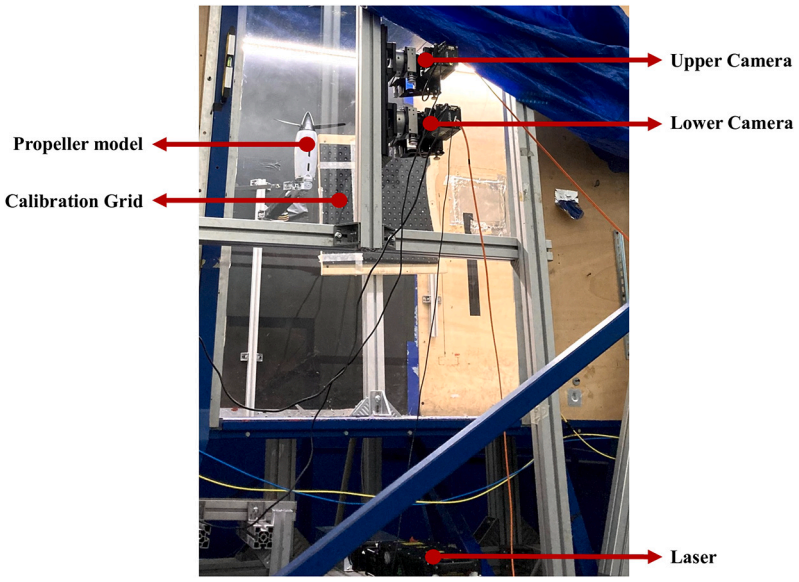

Fig. 4. Layout of the PIV setup.

sion. Details about the accuracy of the PIV measurements are reported in [13]. In particular, considering pulse-separation time and the optical magnification used for the present tests, the maximum in-plane velocity error was below 1% of the maximum in-plane velocity component.

2.4. Wind tunnel test conditions and parameters

The main objective of the experimental campaign was to investigate the performance of tandem propellers when reproducing steady-state points from hover to cruise operations, with focus on the interactional effects on rear propeller. With this aim, a systematic series of tests were performed over several tandem propeller configurations obtained by changing the tilting angle of attack (α_P) of both propellers with same value, thus reproducing a Vahana-like eVTOL architecture during the transition manoeuvre. Moreover, interactional effects obtained with different propellers disks overlap was investigated by changing the vertical distance between the propellers (D_y). In the tandem configuration, the longitudinal distance between the propellers disks was kept constant during the whole campaign and equal to $D_x = 5R$, while vertical offset effects were investigated by considering three different separations $D_y = [0,\ 0.5,\ 1]R$. In particular, front propeller is shifted only downwards to reproduce an Airbus Vahana-like eVTOL architecture. The definition of reference system, propellers relative distances, tilting angle of attack and blades azimuthal angle ψ is shown in Fig. 5.

Wind tunnel test conditions consisted of runs performed with tandem co-rotating clockwise propellers with rotational speed of both propellers controlled to 7050 RPM. This RPM target value was considered to reproduce a typical tip Mach number, i.e. $M_t = 0.325$, of full-scale eVTOL aircraft propellers in cruise flight condition [20,21]. The collective pitch of both the propellers blades was fixed to $\theta = 20.5°$. Tests started with single propeller configuration to obtain reference conditions to evaluate interactional effects in tandem configurations. Single and tandem configurations tests included a range of tilting angles between 0° to 90° with a step of 15°. Different advance ratios i.e. $J = [0.32,\ 0.53,\ 0.75,\ 0.95]$ were considered during the experimental campaign to reproduce the different phases of the transition manoeuvre from take-off to cruise. Advance ratio was modified by changing the wind tunnel free-stream velocity in the test chamber while keeping constant the propellers RPM. An overview of the test conditions and configurations for the performance measurements is reported in Table 1. PIV surveys were performed for a reduced set of tandem propellers configurations only, in order to fit time requirements of the wind

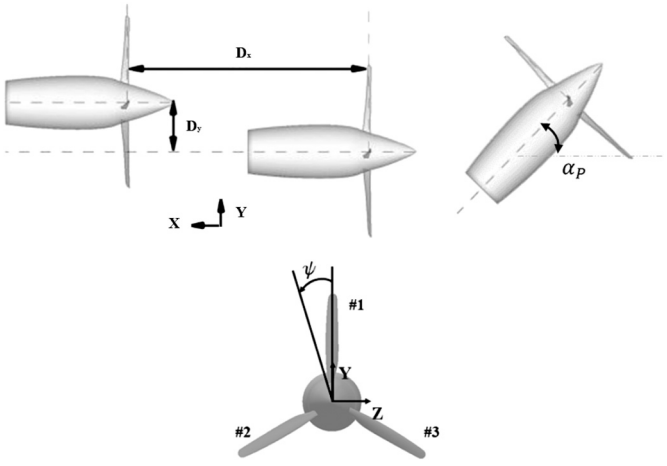

Fig. 5. Schematic of the tandem propeller configuration including definitions of relative distances, tilting angle of attack and blades azimuthal angle of rotation.

Table 1
Summary of test conditions and configurations for performance measurements.

	RPM	J	$\alpha_p[°]$	$D_y[R]$
Single	7050	[0.32, 0.53, 0.75, 0.95]	[0 – 90] step 15	/
Tandem	7050	[0.32, 0.53, 0.75, 0.95]	[0 – 90] step 15	[0, 0.5, 1]

tunnel campaign. Indeed, due to the huge amount of propellers configurations planned in this activity, the present campaign already involved two months of wind tunnel occupancy.

3. Numerical simulations of wind tunnel tests configurations

Numerical simulations were performed using the mid-fidelity aerodynamic solver DUST, developed by Politecnico di Milano [12], to provide insights useful to enhance the physical comprehension of the interactional mechanisms occurring during the reproduce transition configurations of the dual propeller system. DUST is a VPM-based [22,23] solver implementing several numerical elements as lifting lines, surface panels and non-linear vortex lattices. In particular, the wake shed from the trailing edges of lifting bodies is modelled as a panel wake, which

Table 2
Airfoils sections, chord and twist distributions along the propeller blade span.

r/R	chord [m]	twist [deg]	Airfoil
0.24	15.6	24.8	GOE-570
0.32	19.0	15.0	GOE-421
0.39	20.3	9.8	GOE-421
0.47	20.3	6.6	GOE-421
0.55	19.9	4.0	GOE-222
0.62	19.3	2.2	MH-112
0.70	18.5	0.78	GOE-675
0.77	17.5	-0.33	GOE-412
0.85	16.3	-1.07	NACA-4412
0.92	14.9	-1.57	GOE-564
0.97	13.2	-1.40	MH-23
1.00	7.3	-1.24	MH-23

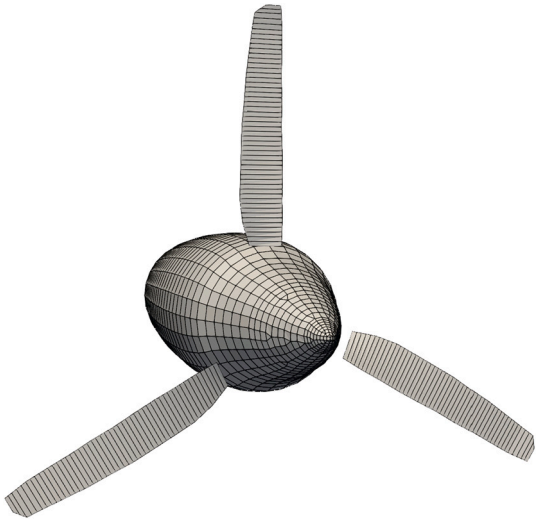

Fig. 6. Propeller model mesh built for DUST simulations.

shares the same spatial discretization that is used to model the lifting bodies and the same formulation as vortex lattice elements in terms of geometry and singularity distribution. When advected downstream, the panel wake is converted into vortex particles released from each section of the modelled lifting body at each time step and then preserved until the end of the simulation. The evolution of wake particles is described by the equation of vorticity dynamics, taking into account the contributions from free-stream and body velocity. The reader is referred to [12] for a complete description of the mathematical formulation of the code. The code was thoroughly validated against experiments and high fidelity CFD for eVTOL configurations [21,24,25] and was successfully used in the recent investigation of tandem propellers interaction in cruise condition [13].

A numerical model of the propeller was built using a CAD model digitally created by means of a 3D scanning of the blade model. A total number of 12 sections were extracted along the span direction. For each section, the airfoil geometry was extracted and the distribution of twist, chord, sweep and dihedral was derived along the blade radial coordinate (r), as reported in Table 2. Blade numerical model was built considering airfoils of the GOE, NACA, and MH series reproducing the sectional geometries derived from the scan. The selected airfoils as well as their blade spanwise position are reported in Table 2. The 2D aerodynamic coefficients of the selected airfoils required for lifting line modelling of the blades were calculated by XFOIL simulations [26] in the range of angles of attack before stall. The Viterna method [27] was used to calculate the post-stall behaviour of the sectional aerodynamic load coefficients in the angle of attack range between $\pm 180°$.

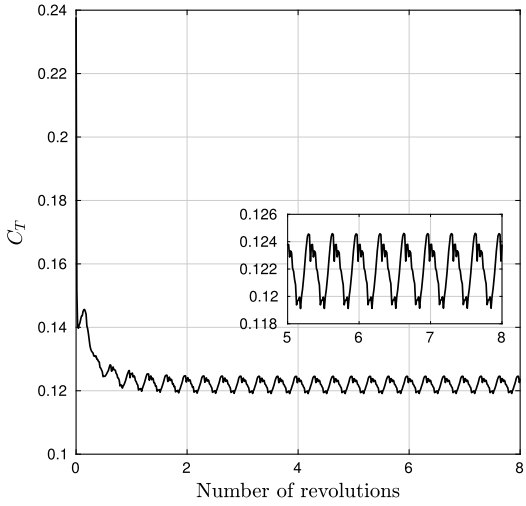

Fig. 7. Thrust Coefficient time history for single propeller configuration at $J = 0.75$ and $\alpha_P = 45°$.

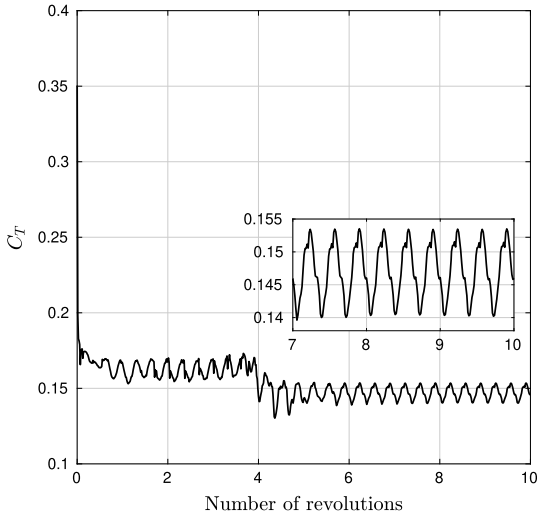

Fig. 8. Thrust Coefficient time history for tandem propeller configuration at $J = 0.53$, $\alpha_P = 60°$ and $D_y = 0$.

An amount of 50 lifting lines in the spanwise direction were used to model each blade. Spinner-nacelle surface was modelled using 1212 surface panels. Blades and spinner-nacelle system geometry could be provided on request to authors. The propeller mesh built for DUST simulations is shown in Fig. 6.

DUST simulations reproduced single and some selected tandem propellers configurations with different tilting angle of attack, as tested during the experiments. For tandem propeller configurations, simulations were performed with propellers blades synchronised in terms of azimuthal angle. The selection of the spatial and time-step discretisation parameters used for the simulations was dictated by a spatial and time-dependence study and validation with experimental results obtained for the single propeller configurations at different tilting angles of attack reported in [28] for the sake of consistency.

Concerning the total simulation time, effectively expressed by the number of overall propeller revolutions performed, this parameter was fixed to obtain whether an approximately steady state condition of the computed loads or a fully periodic oscillation of the same, in case of non-null tilting angle of attack of single propeller configuration as well as for all the tandem interacting test cases. Therefore, in order to properly compute thrust and power coefficients to be compared with ex-

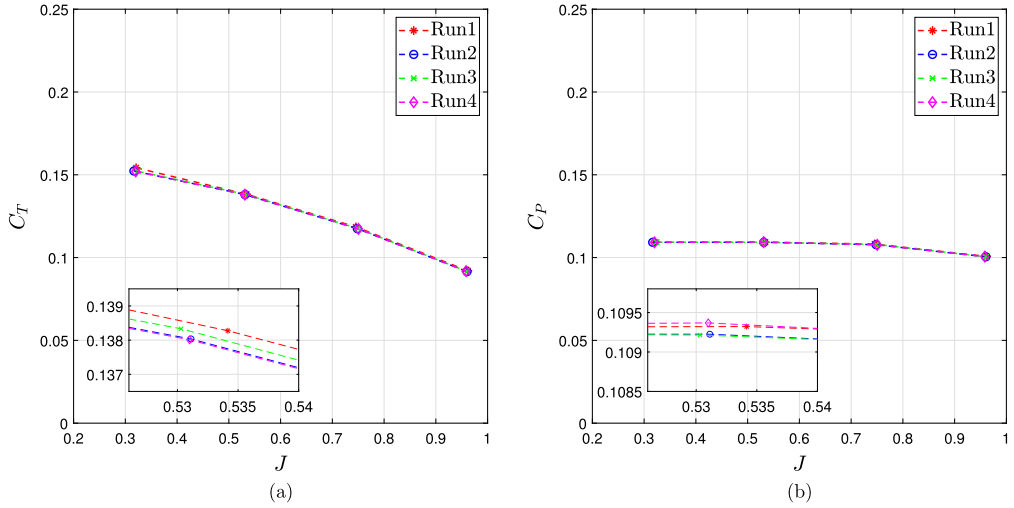

Fig. 9. Loads measurements repeatability: thrust and power coefficients measured in the four repetition runs with single propeller at $\alpha_P = 45°$.

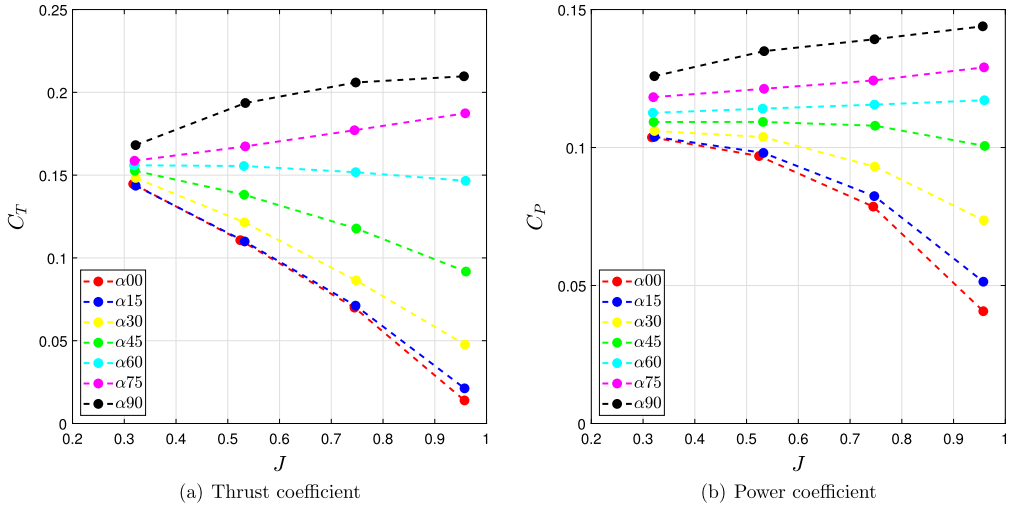

Fig. 10. Thrust and power coefficients curves as function of advance ratio J for the single propeller at different tilting angle of attack.

perimental findings obtained on free-run propellers, the integral loads acting on the propellers were averaged over the last computed three propellers revolutions. As a result, the overall simulation time must be enough to obtain a fully converged solution over at least the last three revolutions. As depicted in Fig. 7, showing the time history of the computed thrust coefficient for a sample configuration with $\alpha_P = 45°$, a number of revolutions equal to eight is sufficient to reach loads convergence for single propeller test cases with non-null tilting angle of attack. Indeed, a fully periodic behaviour over the last three revolutions of interest can be observed particularly from the zoomed view of simulation results depicted in Fig. 7.

Now considering tandem configurations, the number of simulated revolutions were selected in order to reach a periodic trend of the rear propeller loads after the impingement of the wake released by the front one. For the advance ratios involved in the tandem propellers numerical simulations $J = 0.53$ and $J = 0.75$, a total number of ten revolutions were proven to be enough to obtain a fully converged solution, as can be observed from the rear propeller thrust coefficient time history computed for a sample co-axial configuration with $\alpha_P = 60°$ shown in Fig. 8. In particular, the interactional effects of the front propeller wake impinging on rear propeller disk are visible in the drop of thrust coefficient observed after four revolutions, while the zoomed view of simulation results confirmed the fully periodic behaviour of the loads over the last three revolutions of interest.

Simulations of the tandem propeller configurations were thus performed considering a length of 10 propeller revolutions with a time discretization of 5° of blade azimuthal angle. The computational time required to complete a simulation was about 10 and 17 minutes respectively for the single and tandem propellers configurations, by using a workstation with a Dual Intel® Xeon Gold 6230R @2.10GHz processor with 52 physical cores and 2 threads for each core.

4. Results and discussion

Experiments provided a wide amount of data as they explored the whole range of attitudes covered by propellers reproducing a transition manoeuvre from take-off to cruise. In the present section, the main results of both experimental and numerical activities are discussed considering the aerodynamic performance of the single propeller first. Then, results for tandem propellers configurations are analysed by considering three different phases characterising the transition manoeuvre, i.e the initial phase performed at low speeds and high tilting angles of attack, the last phase characterised by higher speeds and lower tilting angles of attack and the intermediate phase to complete the overview.

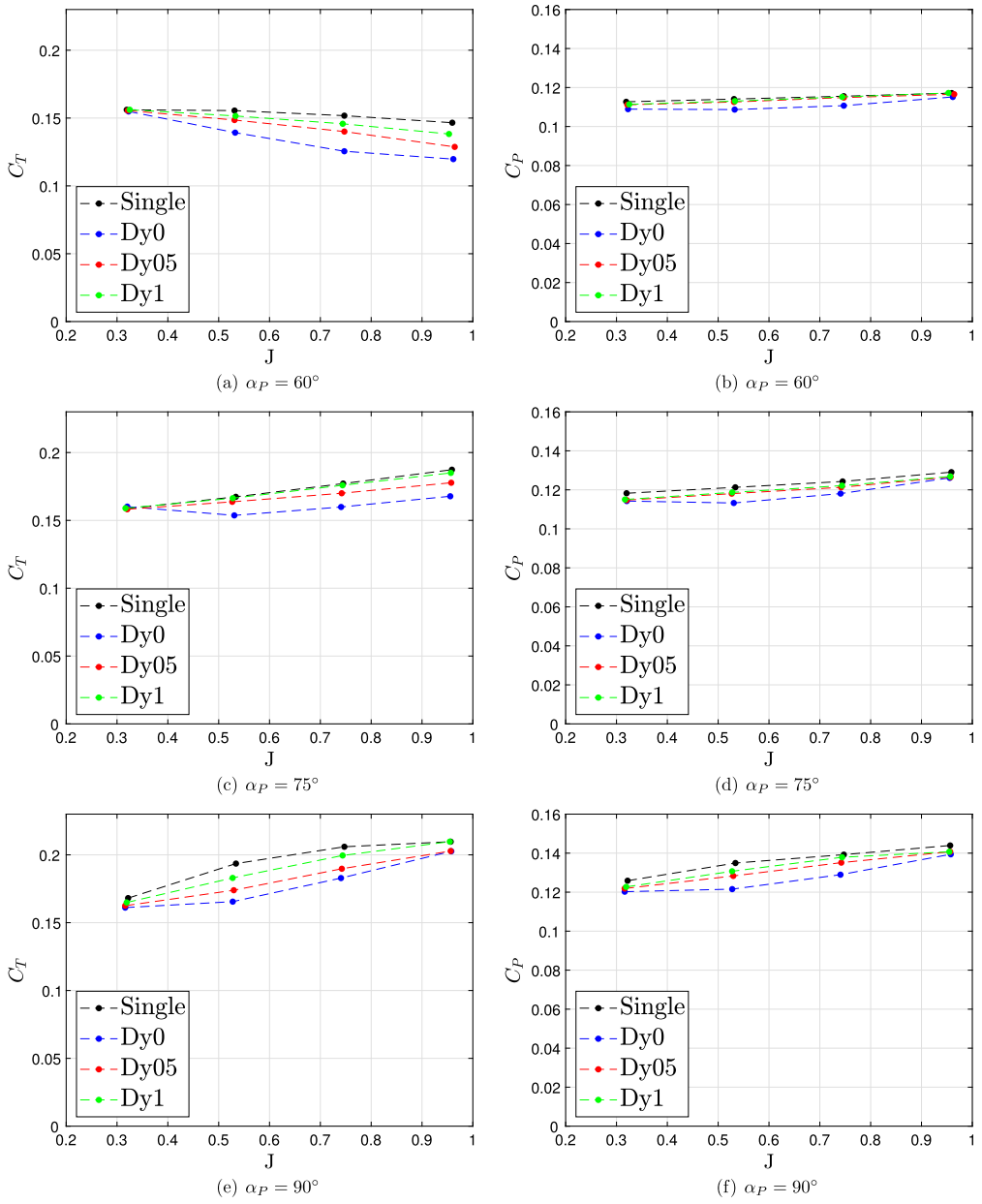

Fig. 11. Comparison of the thrust and power coefficients curves measured for the rear propeller in tandem at high tilting angles of attack for different vertical separation distances.

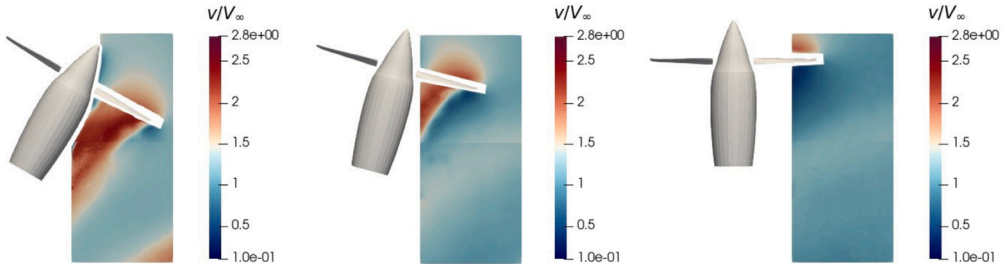

Fig. 12. In-plane velocity magnitude measured by PIV around the rear propeller in tandem for co-axial configuration at different tilting angle of attack, $J = 0.32$.

4.1. Single propeller analysis

Before presenting the experimental results obtained at different tilting angle of the propeller an analysis of loads measurements accuracy is provided in the following. Fig. 9 shows the experimental thrust and power coefficients curves collected during the four measurements repetitions performed for each point with single propeller at $\alpha_P = 45°$, which, without any loss of generality, can be chosen as an example to

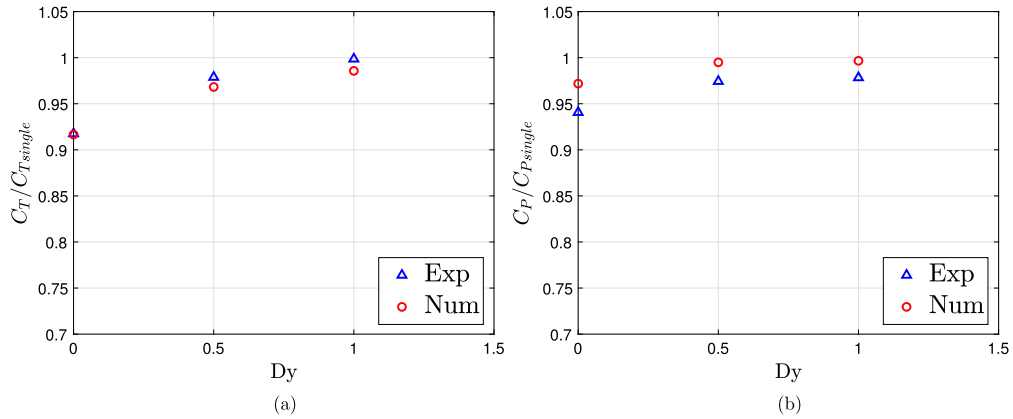

Fig. 13. Comparison of the experimental and numerical (DUST) thrust and power coefficients evaluated for the rear propeller as function of vertical distance D_y in tandem configuration with $\alpha_P = 60^\circ$ and $J = 0.53$.

be representative for the behaviour of all other configurations, including tandem configurations. A zoom window is included in the graph to appreciate the negligible differences between the four curves, thus highlighting an excellent repeatability of the measurements. Therefore, error bars related to standard deviation of the repeated loads measurements is not plotted in the following figure showing the mean values of the measured C_T and C_P.

Fig. 10 shows thrust and power coefficients curves measured for the single propeller at all the investigated tilting angles of attack. The performance curves measured at zero tilting angle of attack differed from the ones evaluated in the previous work [14] using the same set up due to the different pitch angle used for the propeller blades in this activity, i.e. $\theta = 20.5^\circ$ rather than $\theta = 26.5^\circ$. The curves behaviour shows a good consistency with the findings obtained by [6] using a similar test set up. The performance curves tend to diverge increasing advance ratio, which leads to a significant change in the effective angle of attack of the blades over the propeller disk. Furthermore, a decreasing trend of the curves was found with respect to advance ratio for $\alpha_P < 60^\circ$, while an increasing trend is observed for $\alpha_P = 75^\circ$ and 90°.

The change of the curves slope for high propeller tilting angles can be explained considering the axial induced velocity impinging on propeller disk at the different attitudes, as described by Ortun et al. [29] and Stokkermans et al. [18]. Indeed, for a propeller at incidence the wake shed by the blade in the advancing side of the disk is stronger compared to the wake released by the blade in the retracting side. As a result, the induced velocity field is stronger in the proximity of $\psi = 0^\circ$ rather than near $\psi = 180^\circ$, leading to a clockwise rotation of the axial induced velocity over the disk. This effect provides a phase lag [29] of the blades effective angle of attack, therefore also of the generated thrust. As a consequence, the loads generated are higher in the propeller disk region near $\psi = 180^\circ$ with respect to $\psi = 0^\circ$. The stronger is the imbalance between the two sides of the disk, the larger is the magnitude of phase lag. The imbalance become larger both increasing propeller tilting angle of attack and advance ratio.

4.2. Tandem propellers analysis

4.2.1. Initial phase of transition

In the first phase of transition, Vahana-like eVTOLs flight conditions are typically characterised by low air speeds and high propellers tilting angles of attack. Thus, this subsection shows experimental results obtained for $\alpha_P = 60^\circ$, $\alpha_P = 75^\circ$ and $\alpha_P = 90^\circ$. Fig. 11 shows thrust and power coefficients measured for the rear propeller at different vertical separation distances, compared with single propeller results.

The first appreciable result is the effect of vertical separation between propellers on the trends of rear propeller loads coefficient curves. The largest detrimental effects are observed for co-axial propellers

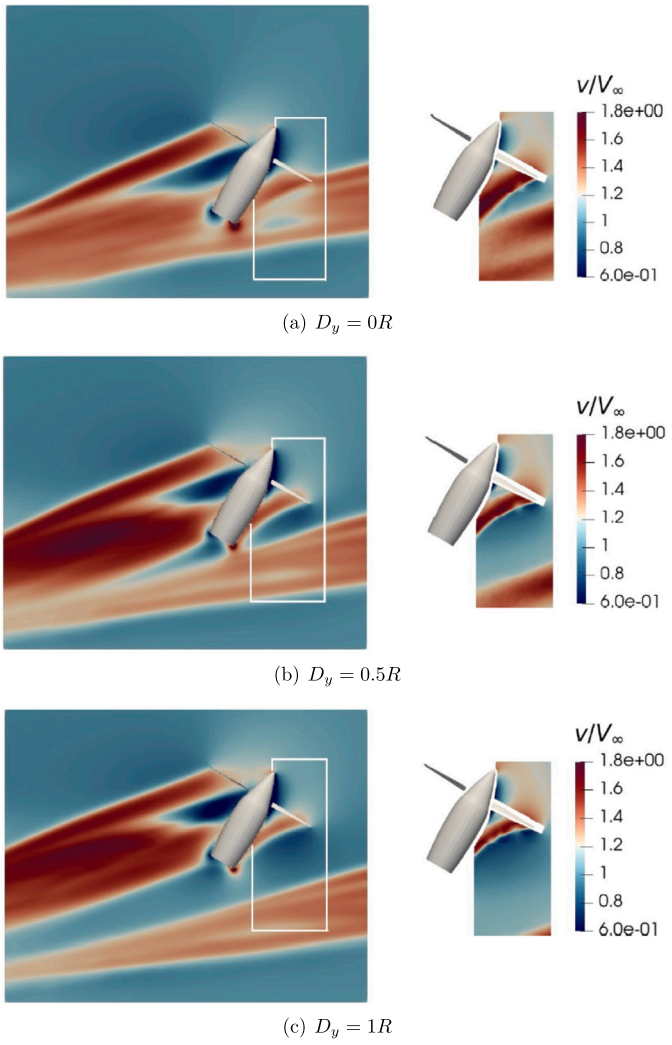

Fig. 14. Comparison between the in-plane velocity magnitude evaluated by DUST (left) and PIV (right) for the tandem propellers configurations with $\alpha_P = 60^\circ$ and $J = 0.53$. PIV area of investigation is confined in numerical flow field by a white line.

($D_y = 0$) at all the considered propeller tilting angles of attack. In particular, for $\alpha_P = 60^\circ$ and $\alpha_P = 75^\circ$, rear propeller thrust and power losses evaluated between $D_y = 0.5R$ and $D_y = 1R$ are lighter with respect to the variations occurring between $D_y = 0$ and $D_y = 0.5R$ configurations.

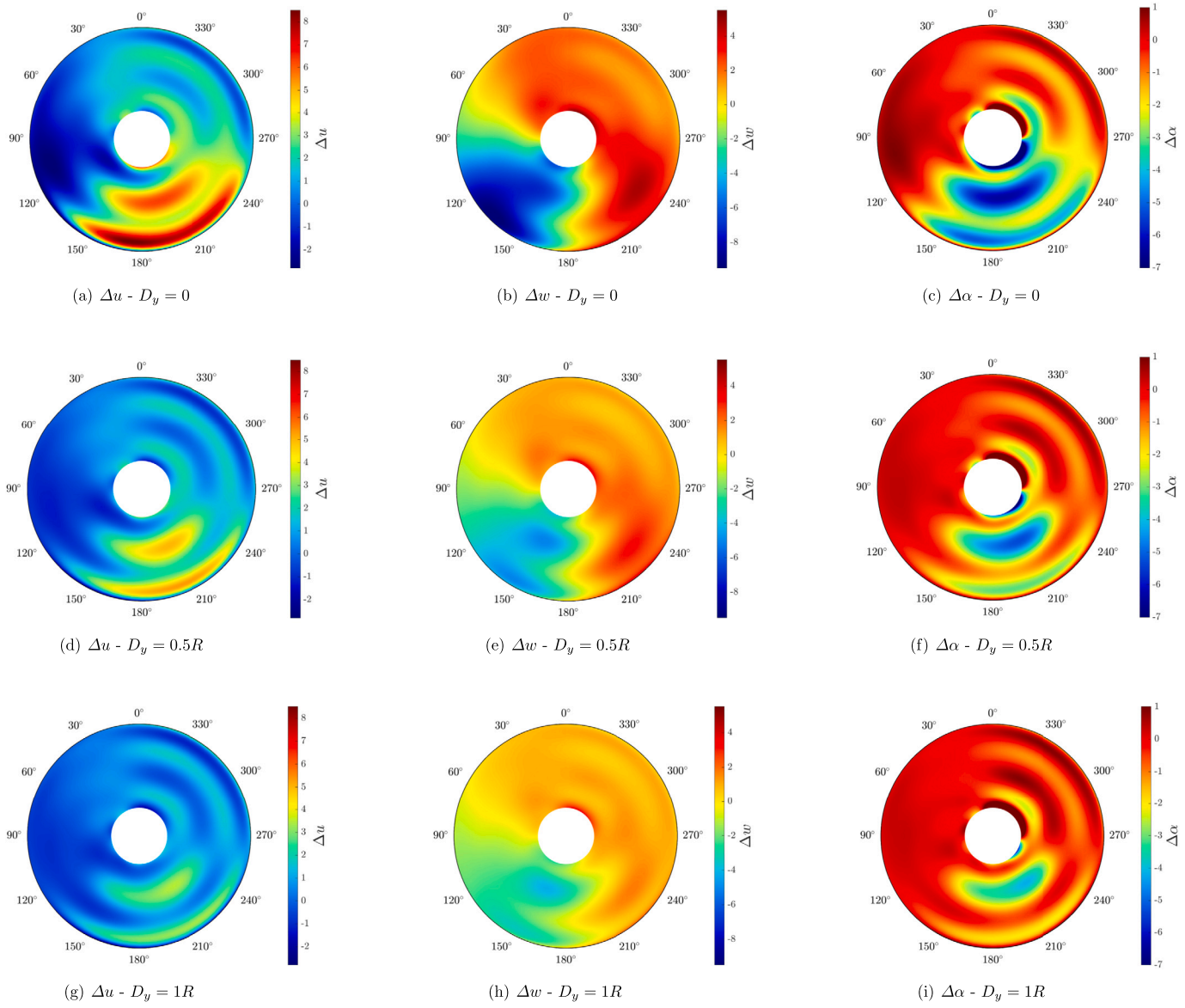

Fig. 15. Variations of the axial velocity $\Delta u = u_{rp} - u_{sp}$ [m/s], tangential velocity $\Delta w = w_{rp} - w_{sp}$ [m/s] and effective angle of attack $\Delta\alpha = \alpha_{rp} - \alpha_{sp}$ [deg] computed by DUST for the rear propeller blade along azimuthal angle ψ with respect to the single propeller configuration for $\alpha_P = 60°$ and $J = 0.53$.

This behaviour highlights a rapid decrease of interactional effects while shifting the rear propeller upwards. On the other hand, for $\alpha_P = 90°$ a more linear trend concerning performance losses variations can be observed among the different vertical separation distances tested.

Now considering the performance curves trend with respect to advance ratio, a decrease of the $C_T - J$ curve slope with respect to single propeller case is apparent, particularly for $\alpha_P = 60°$. For both $\alpha_P = 60°$ and $\alpha_P = 75°$ performance curves tend to diverge by increasing advance ratio, as the higher free-stream velocity is responsible of a downstream dragging of front propeller wake, providing an increase of aerodynamic interaction between the two propellers. A different behaviour is instead found for $\alpha_P = 90°$, where loads curves tend to converge for $J = 0.32$ and $J = 0.95$, thus highlighting a substantial absence of interactional phenomena in this configuration.

Focusing the attention on results obtained at the lowest advance ratio tested, i.e. $J = 0.32$, a relevant feature is the collapsing behaviour of the loads curves, thus revealing almost negligible interference effects between front propeller slipstream and rear propeller disk. Flow field surveys obtained by PIV confirm this latter outcome, as illustrated in Fig. 12 showing the averaged in-plane velocity magnitude measured around the rear propeller for co-axial configuration at different tilting angle of attack. Indeed, only for the smallest tilting angle $\alpha_P = 60°$ a quite small portion of the front slipstream is visible in the lower right corner of the cameras framing, further from rear propeller disk.

A more detailed investigation supported by DUST numerical simulations results is then provided for a test configuration at higher advance ratio, i.e. $\alpha_P = 60°$ and $J = 0.53$, showing effective detrimental effects in terms of rear propeller performance due to the higher interaction between the front and rear propeller slipstreams. Fig. 13 shows the comparison of experimental and numerical loads coefficients evaluated for the rear propeller as function of vertical distance D_y. In particular, rear propeller thrust and power coefficients are shown as ratio with respect to the corresponding single propeller values to highlight the interactional effects in tandem configuration.

Fig. 13 shows a quite good correspondence between the experimental and numerical data. Going into details, a slight underestimation of thrust coefficient is observed for non-null vertical distances, while a slight underestimation of C_P losses in the order of few percents is observed for all the three analysed configurations. This comparison highlights the reliability of the numerical solver to capture the aerodynamic

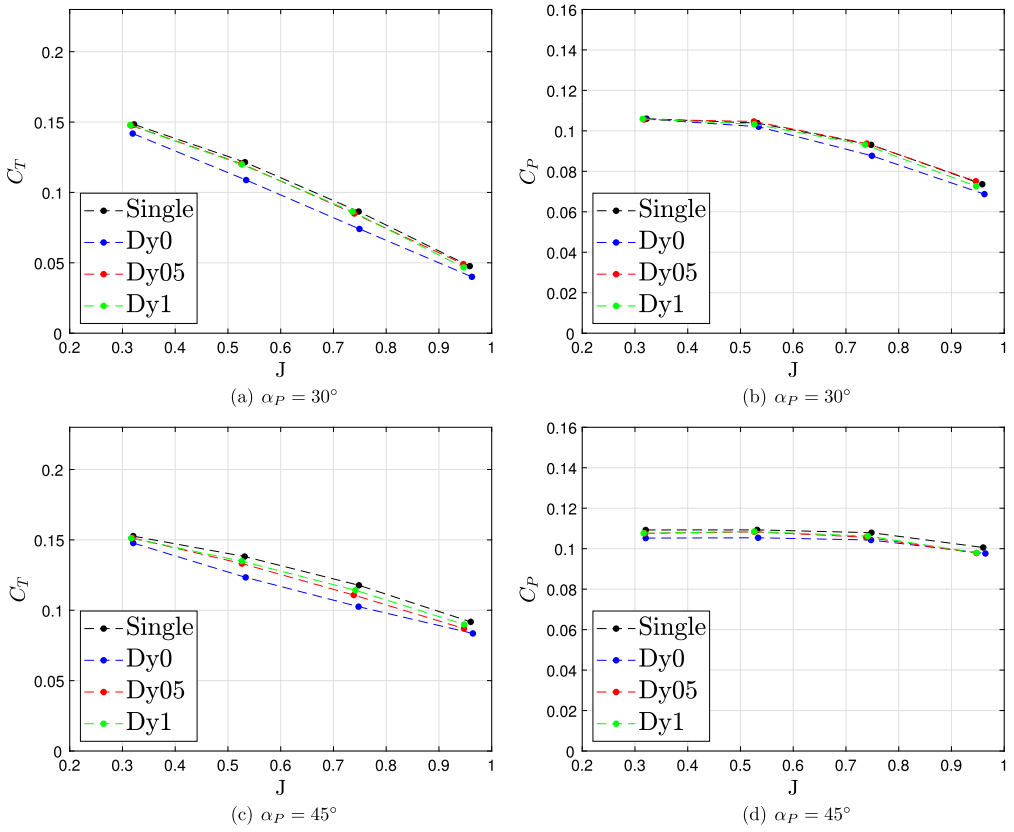

Fig. 16. Comparison of the thrust and power coefficients curves measured for the rear propeller in tandem at intermediate tilting angles of attack for different vertical separation distances.

interaction effect on the rear propeller in tandem. Indeed, numerical findings confirm the higher detrimental effects observed for the coaxial configuration for both thrust and power coefficients, lying below 10% of the single propeller values. Increasing vertical separation, the rear propeller resumes almost the performance evaluated for the single propeller.

Further validation of the numerical model is provided by the comparison of flow fields reported in Fig. 14, showing the in-plane velocity magnitude evaluated by DUST and PIV at different vertical distances. Flow field analysis confirms that higher interactional effects are present for the co-axial configuration, as rear propeller is more influenced by front propeller wake. Comparison with numerical results shows that DUST captures the overall behaviour of the flow field, particularly the downward shift of the front propeller wake with increasing vertical distance. Nevertheless, numerical results shows that front propeller wakes are less deflected with respect to experiments. This leads to observe from numerical calculations a larger portion of the front propeller wake inside the lower region of the PIV area of interest for all the three configurations tested. Moreover, as DUST relies on a mathematical formulation based on a potential method, separation and recirculation regions that reasonably arise downstream the rear propeller nacelle are not captured. Generally, flow field comparison confirms the capability of DUST to reproduce the flow physics around rear propeller occurring for this tandem configuration with some differences with respect to front propeller wake deflection impinging rear propeller disk. Simulations results are used to support a physical explanation of the performance losses observed on the rear propeller. With this aim, polar plots depicted in Fig. 15 show the variations of axial velocity Δu, tangential velocity Δw and the local effective angle of attack $\Delta\alpha$ experienced by the rear propeller blade in tandem configuration along the last computed revolution with respect to the corresponding single propeller values.

For what concerns the coaxial configuration, due to the high tilting angle of the propellers and a quite limited advance ratio, even if a direct impingement of the front propeller slipstream on the rear propeller disk is limited (see Fig. 14(a)), the highly deflected wake coming from the front propeller provides the arise of a non negligible vertical velocity component directed downwards, thus increasing the deflection of rear propeller inflow with respect to single propeller configuration. This effect resembles a reduction of rear propeller effective tilting angle of attack, thus leading to a weaker disk imbalance between the advancing and the retracting sides of propeller disk with respect to single propeller configuration.

The variations of axial and tangential velocity components experienced by rear propeller blade reflect this behaviour, as shown in Fig. 15(a) and Fig. 15(b). Specifically, a decrease of axial velocity is found on the advancing side of the disk around $\psi = 90°$, while an increase is found in the first half of the retracting side of the disk. A reduction of the effective tilting angle of attack produces also a decrease of the tangential velocity component experienced by the rear propeller blade on the advancing side of the disk, as evidenced by the negative Δw in the region $90° < \psi < 180°$, while an increase of w is provided in the retracting half of the disk. The combination of both velocity components variations determine the modification of the local angle of attack experienced by the rear propeller blade. In particular, $\Delta\alpha$ contours depicted in Fig. 15(c) shows the predominant role of the axial component variation on the effective angle of attack with respect to tangential velocity component. Indeed, $\Delta\alpha$ polar plot mainly reflects the topology of Δu one, showing a robust decrease of blade local angle of attack in the disk regions where positive axial velocity variations occur, while slight increases of local angle of attack occur on the advancing side of the disk where blade experiences negative axial velocity variations. This behaviour of the local angle of attack over the entire disk supports the average thrust decrease measured for the rear propeller in tandem with respect to single propeller configuration.

Now considering the effects of vertical separation increase between front and rear propellers, the first evidence of the comparison with

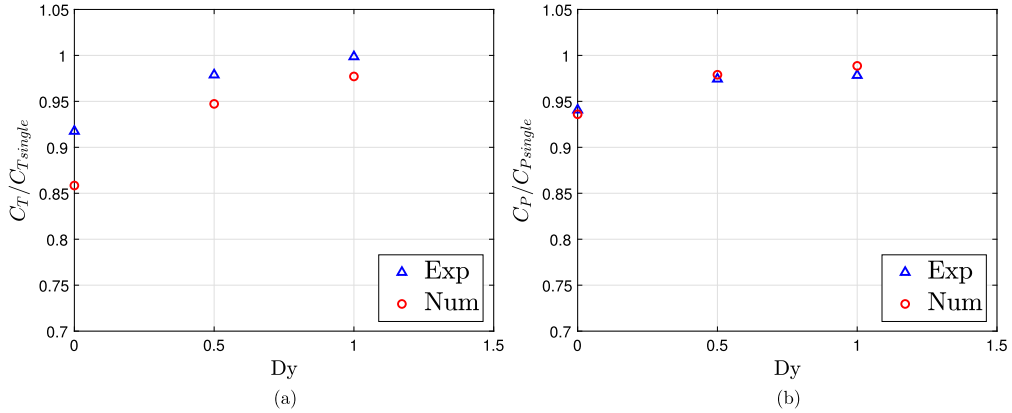

Fig. 17. Comparison of the experimental and numerical (DUST) thrust and power coefficients evaluated for the rear propeller as function of vertical distance D_y for tandem configuration with $\alpha_P = 45°$ and $J = 0.53$.

co-axial results is the reduced impact of the effects related to inflow modifications introduced by the presence of front propeller. In particular, the sectional distributions of the investigated quantities variations shown in Fig. 15 for $D_y = 0.5R$ and $D_y = 1R$ present the same pattern observed for coaxial configuration, but characterised by a gradually decreasing intensity. As can be expected, the downward shift of the front propeller brings its slipstream further from the rear propeller disk, thus inducing a lower vertical velocity component to the rear propeller inflow. As a consequence, the impact in terms of effective angle of attack reduction is smaller and lower variations are found on rear propeller disk. This feature is coherent with performance measurements highlighting that rear propeller performance gradually approaches the single propeller one when the vertical distance between the tandem propellers is increased up to $D_y = 1R$.

4.2.2. Intermediate phase of transition

In this subsection experimental results are presented for intermediate tilting angles of the propellers, i.e. $\alpha_P = 30°$ and $\alpha_P = 45°$. Fig. 16 shows thrust and power coefficients measured for the rear propeller with different vertical separation distances compared with single propeller results. Differently from what observed at higher tilting angles of attack, the slope of the curves remains very similar to the one measured for the single propeller, thus detrimental effects on rear propeller appear to be quite constant over the entire range of investigated advance ratios. In particular, thrust differences are slightly more pronounced for $J = 0.53$ and $J = 0.75$. Additionally, the increment of D_y is quite more effective in reducing thrust losses when the propeller angle of attack is set to $\alpha_P = 30°$ rather than for the case with $\alpha_P = 45°$.

Now considering interactional effects of C_P, the rear propeller is not significantly affected by the front one, particularly for $J = 0.32$ and $J = 0.53$, while larger differences can be observed for higher advance ratios. The increase of vertical distance leads to almost negligible interactional effects for both the tilting angles of attack considered in this phase. To better investigate the physics of the interaction in this intermediate transition phase, once again DUST simulations results are used for a single selected configuration, i.e. characterised by $\alpha_P = 45°$ and $J = 0.53$. The ratios of thrust and power coefficients evaluated by experiments and simulations on rear propeller with respect to single propeller configuration are compared in Fig. 17.

As observed for the configuration with $\alpha_P = 60°$, both C_T and C_P experimental curves trends are captured by DUST. Nevertheless, an overestimation of thrust losses is observed for numerical calculations that increases by reducing the vertical distance between propellers disks to reach the highest difference of about 7% for co-axial configuration. On the other hand, a quite good matching between power coefficient values is obtained for all the tandem configurations tested. As done for the previous investigated condition, the comparison of the in-plane velocity magnitude evaluated by DUST and PIV at different vertical distances is then shown in Fig. 18.

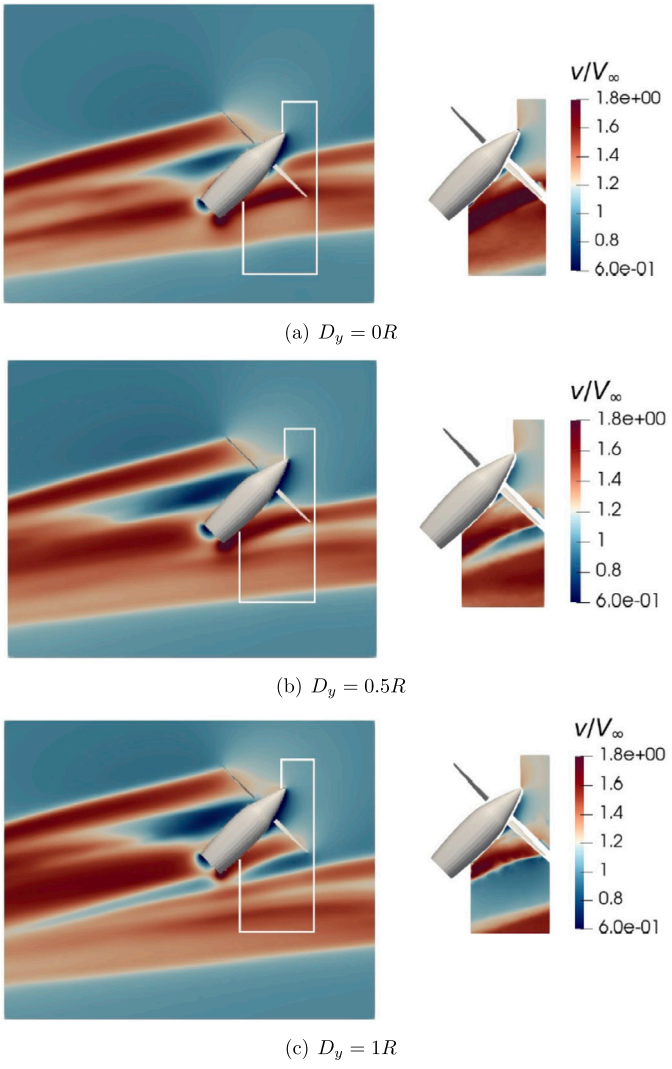

Fig. 18. Comparison between the in-plane velocity magnitude evaluated by DUST (left) and PIV (right) for the tandem propellers configurations with $\alpha_P = 45°$ and $J = 0.53$. PIV area of investigation is confined in numerical flow field by a white line.

Even for this case, numerical simulations capture the overall behaviour of the propellers wakes with a slight mismatch of front pro-

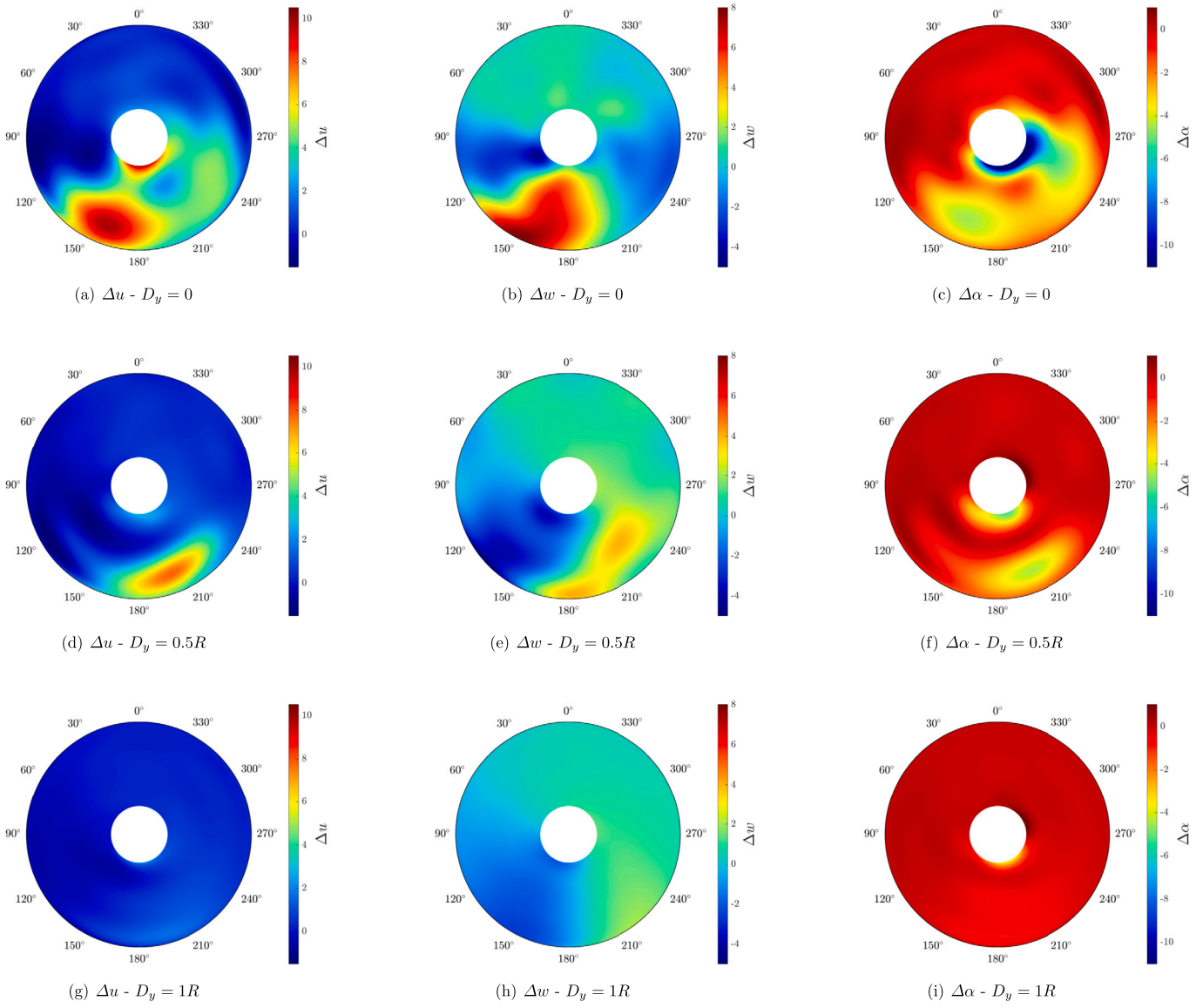

Fig. 19. Variations of the axial velocity $\Delta u = u_{rp} - u_{sp}$ [m/s], tangential velocity $\Delta w = w_{rp} - w_{sp}$ [m/s] and effective angle of attack $\Delta\alpha = \alpha_{rp} - \alpha_{sp}$ [deg] computed by DUST for the rear propeller blade along azimuthal angle ψ with respect to the single propeller configuration for $\alpha_P = 45°$ and $J = 0.53$.

peller positioning inside the PIV area of interest. Also the effects of the vertical separation are captured with a slight mismatch in terms of slipstream intensity. In particular, in the coaxial configuration the lower half of the rear propeller disk is affected by the upper part of the front propeller slipstream, thus supporting the highest interactional effects observed from loads measurements in this configuration. Further support to physical interpretation is provided by DUST results by using the polar plots presented in Fig. 19, as done for the configuration analysed in the last phase of the transition.

Considering the co-axial configuration, Fig. 19(a) evidences that front propeller slipstream affects only the lower half part of rear propeller disk. Again, Δu magnitude reflects the intensity of the impacting wake, which is found to be higher in the region corresponding to the advancing side of the front propeller disk, net of a certain amount of phase lag related to propeller tilting angle. The upper part of the rear propeller disk appears instead to be almost unperturbed, showing negligible u variations.

For what concerns Δw distribution shown in Fig. 19(b), the pattern observed on rear propeller disk is related to the combination of two effects. Indeed, an increase of horizontal velocity in the region of wake impingement provides an increase of tangential velocity w in the advancing side and a decrease in the retracting one in this area. Moreover, the inflow of the rear propeller is influenced by the arise of a vertical velocity component directed downwards, as discussed earlier due to the tilting angle. These effects provide a negative variation of the tangential velocity w in the advancing side of rear propeller disk mainly visible in the region $90° < \psi < 120°$ and around $\psi = 270°$ for the retracting side, while an increase of w is observed for $120° < \psi < 180°$. As a consequence of the combination of the two velocity components variations, the local blade effective angle (see Fig. 19(c)) is not subject to appreciable variation in the upper half of the disk, not interested by front slipstream impingement, while for $130° < \psi < 180°$ the detrimental effects caused by the highly positive Δu are mitigated by the positive variation of the tangential velocity component. On the other hand, for $240° < \Psi < 270°$, the combination of a positive Δu and a negative contribution of Δw produces a slight negative variation of the effective angle of attack experienced by rear propeller blades. As expected, a small portion of the rear propeller disk is affected by local angle of attack reduction with respect to single propeller configuration, thus leading to the small thrust losses measured for this condition.

By increasing the vertical distance between propellers, the interactional effects become lower, thus reducing the variations of the sectional

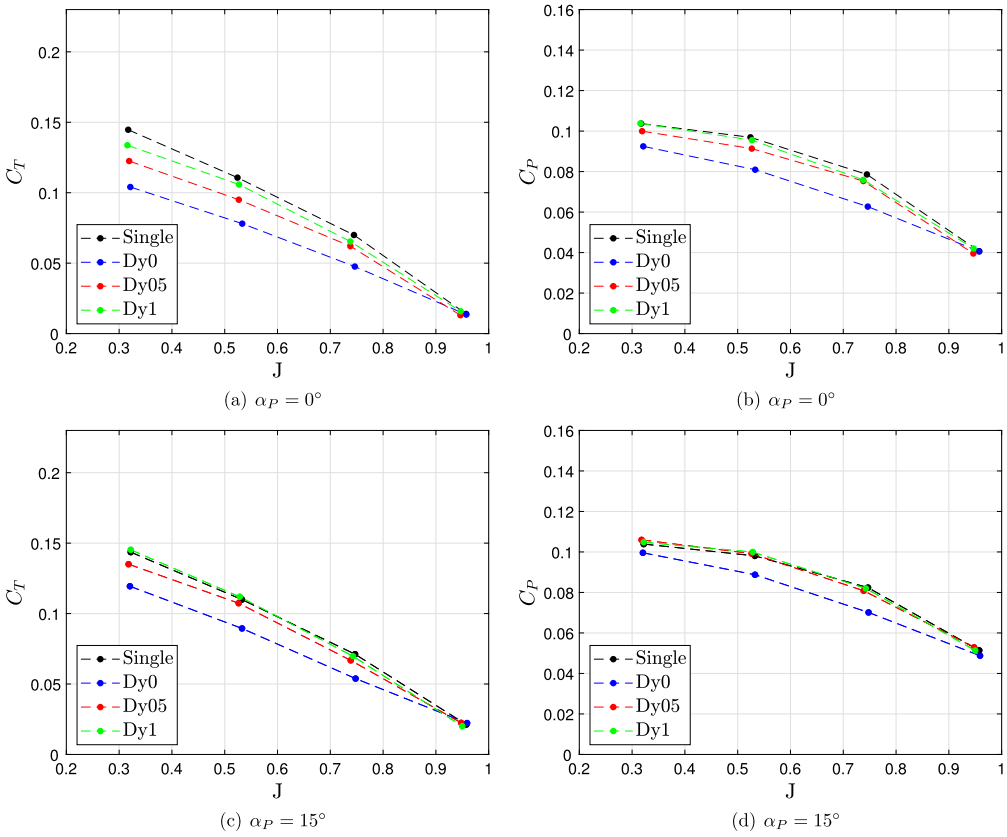

Fig. 20. Comparison of thrust and power coefficients curves measured for the rear propeller in tandem at low and null tilting angles of attack for different vertical separation distances.

features observed in the polar plots. Indeed, increasing the vertical distance up to $D_y = 1R$, the distribution of axial velocity variations over the propeller disk becomes negligible, as evidenced by Fig. 19(g), while some small variations with respect to single propeller condition is still observed. These effects combination leads to an almost full recovery of rear propeller performance reached in this configuration, as supported by blade local angle of attack variation shown in Fig. 19(i).

4.2.3. *Last phase of transition*

Last phase of transition to airplane mode of a tilt-wing eVTOL is characterised by high speeds and low propellers tilting angles of attack. In this subsection experimental results are presented for the lowest tandem propellers tilting angle tested, i.e. $\alpha_P = 15°$, as well as for $\alpha_P = 0°$ for a direct comparison with cruise flight condition. Fig. 20 shows thrust and power coefficients measured for rear propeller at different vertical separation distances compared with single propeller results.

Analogously to what found during last phase of transition flight conditions, the higher performance losses for rear propeller are observed for co-axial configuration, while increasing the vertical distance the rear propeller almost approaches the single propeller performance. On the other hand, in the present conditions the trend of performance curves as function of advance ratio is opposite with respect to what observed in the last phase of transition conditions. Indeed, in this case the rear propeller performance curves tend to converge at high advance ratio. As a matter of fact, with a small angle of attack the front slipstream is quite less deflected and a larger portion of the rear propeller disk is affected by the impingement of the front propeller slipstream. Moreover, the higher performance losses obtained at low advance ratio are related to the stronger slipstream investing the rear propeller related to the higher thrust generated by front propeller in these conditions. On the other hand, at high advance ratio, i.e. $J = 0.95$, the front propeller works near to windmill conditions, thus generating a very low amount of thrust and a consequent much weaker slipstream. Hence the rear propeller, even if fully invested by the front wake, experiences a very small modification of inflow conditions, thus experiencing negligible variations of loads with respect to single propeller condition.

As previously done, discussion considering numerical and experimental results is focused on a single condition that better reproduce an eVTOL in the last phase of the transition, i.e. characterised by $\alpha_P = 15°$ and a higher advance ratio $J = 0.75$. The ratios of thrust and power coefficients evaluated by experiments and simulations on rear propeller with respect to single propeller configuration are compared in Fig. 21. The increasing loss of both C_T and C_P observed by experiments by decreasing the vertical distances between propellers disks are captured by DUST. Nevertheless, a certain mismatch between experimental and numerical values of both C_T and C_P is observed for the test case with $D_y = 0.5R$, where differences between 5% and 10% are found. The main difference with respect to the flight conditions analysed before is that for low propellers tilting angle of attack the performance losses obtained in co-axial configuration are quite higher, reaching values in the order of 25% and 15% respectively of single propeller thrust and power coefficients.

Further insights of flow physics representation is highlighted in Fig. 22, showing the comparison of the in-plane velocity magnitude evaluated by DUST and PIV at different vertical distances. For this flight condition PIV set up enabled to observe a smaller area of investigation focused on the lower wake region of rear propeller. However, DUST results can further provide flow physics insights on a wider area around rear propeller enabling to visualise flow fields differences for the three vertical distances tested. In particular, DUST shows to capture the higher intensity of rear propeller wake obtained for the co-axial configuration due to the complete impingement of the front propeller slipstream. This leads to an higher accelerated flow region past the rear propeller disk with respect to the configurations with vertical distance

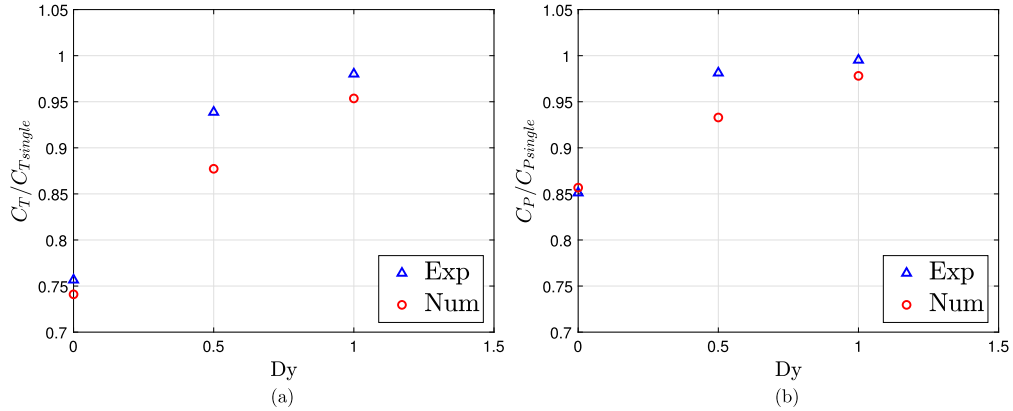

Fig. 21. Comparison of the experimental and numerical (DUST) thrust and power coefficients evaluated for the rear propeller as function of vertical distance D_y for tandem configuration with $\alpha_P = 15^\circ$ and $J = 0.75$.

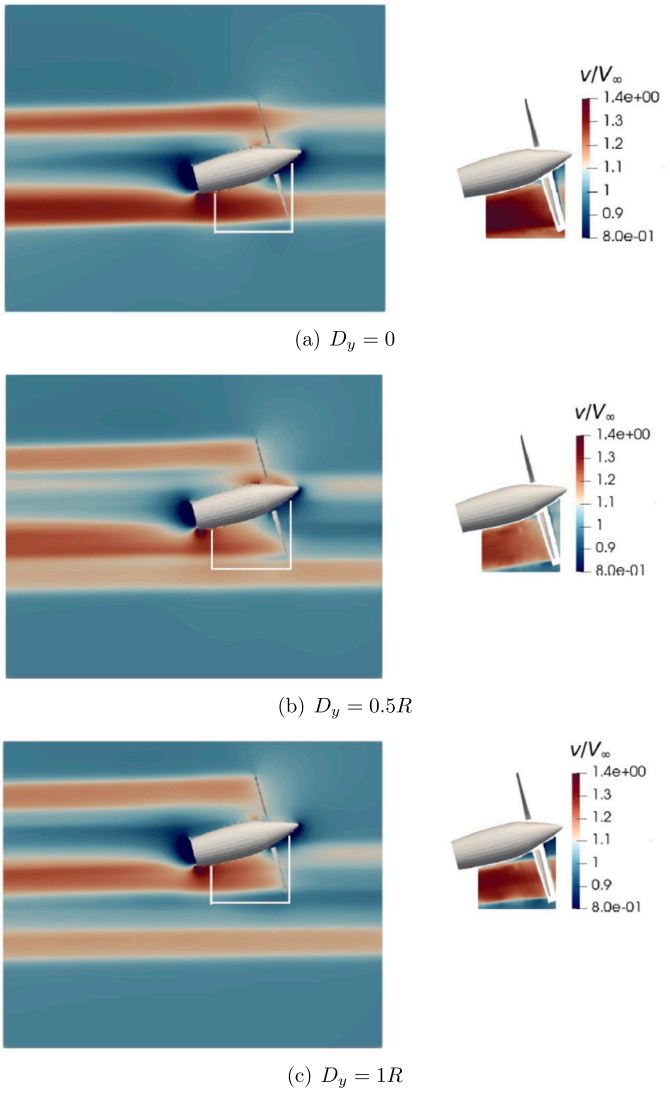

Fig. 22. Comparison between the in-plane velocity magnitude evaluated by DUST (left) and PIV (right) for the tandem propeller configurations with $\alpha_P = 15^\circ$ and $J = 0.75$. PIV area of investigation is confined in numerical flow field by a white line.

between the propeller disks. For $D_y = 0.5R$, the upper region of front propeller wake impinges on the nacelle spinner and is directed towards the higher half of rear propeller disk, while the lower wake region withdraws from the rear propeller inflow, sensibly reducing the region of the disk affected by wake interaction. For $D_y = 1R$, the upper region of front propeller slipstream now affects only the lower side of rear propeller disk, thus providing a significant decrease of the overall detrimental effects related to the interaction. Moreover, all numerical flow fields highlight the different intensity of the lower and upper parts of front slipstream produced as a consequence of phase lag [29].

Again, as done for the previous test cases analysis, the variations of blade sectional velocities and local angle of attack computed by DUST with respect to single propeller is shown in Fig. 23 for the configuration with $\alpha_P = 15^\circ$ and $J = 0.75$. For co-axial configuration, the axial velocity polar plot illustrated in Fig. 23(a) shows a non-symmetric behaviour, as the rear propeller is invested by a non-uniform slipstream coming from the front propeller due to the intrinsic imbalance between the advancing and retracting sides of propeller disk related to tilting angle. Indeed, a positive axial velocity variation is found for $60^\circ < \psi < 210^\circ$, while an almost negligible variation is observed for $270^\circ < \psi < 360^\circ$. Additionally, the Δu plot disk shows a certain rotation related to phase lag of the front propeller wake, almost investing the rear propeller disk. The variation of tangential velocity is related to the combination of the effects provided by the swirl and vertical velocity components provided by the deflected front propeller slipstream investing the rear propeller disk. This leads to a complex shape of the w variations distribution on rear propeller disk, as shown in Fig. 23(b). Nevertheless, the interactional effect on blade local tangential velocity is quite lower with respect to axial velocity one. Indeed, the effective angle of attack variations reported in Fig. 23(c) reflects the same distribution found for u variation, showing negative $\Delta\alpha$ where Δu is positive, i.e. for $60^\circ < \psi < 210^\circ$, while negligible variations occur for $240^\circ < \Psi < 360^\circ$, where Δu is substantially null.

Considering the effects of vertical separations between propellers, for the configuration with $D_y = 0.5R$ the lower half of rear propeller disk advancing side is affected by a variation of axial velocity (see Fig. 23(d)), while for $D_y = 1R$, as the lower portion of the rear propeller disk is affected by the upper and weaker region of the front propeller slipstream, u variations are smaller in the same azimuthal disk area (see Fig. 23(g)). For what concerns the distribution of tangential velocity variation, $D_y = 0.5R$ case reveals a quite complex behaviour related to the interaction of the middle region of front propeller slipstream (see Fig. 23(g)), while for $D_y = 1R$ the interaction between the upper region of front propeller wake and the lower portion of rear propeller disk provides a positive Δw clearly visible in Fig. 23(h). Generally, for both vertical separations, the variations of effective angle of attack reflect the distributions of Δu and show a significant decrease of $\Delta\alpha$ in the regions of impingement of front propeller slipstream. Comparing Fig. 23(f) and Fig. 23(i), as the regions affected by front propeller slipstream get increasingly smaller, detrimental effects on rear propeller

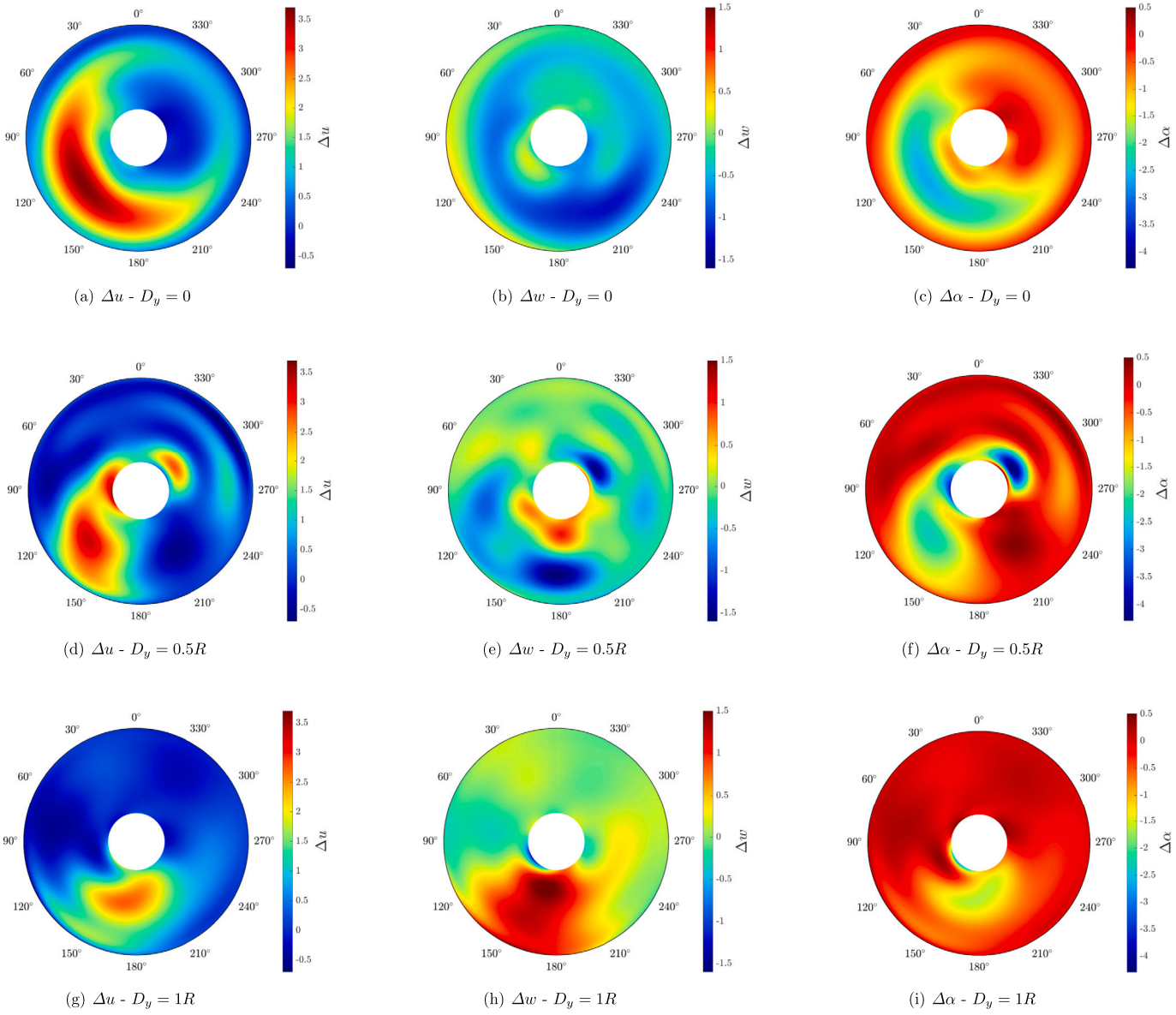

Fig. 23. Variations of the axial velocity $\Delta u = u_{rp} - u_{sp}$ [m/s], tangential velocity $\Delta w = w_{rp} - w_{sp}$ [m/s] and effective angle of attack $\Delta\alpha = \alpha_{rp} - \alpha_{sp}$ [deg] computed by DUST for the rear propeller blade along azimuthal angle ψ with respect to the single propeller configuration for $\alpha_P = 15°$ and $J = 0.75$.

thrust generation related to interactional mechanisms decrease by increasing the vertical separation.

5. Conclusions

Aerodynamic interaction occurring between tandem propellers during the transition manoeuvre typical of an eVTOL flight envelope was deeply investigated and analysed both through experimental and numerical activities. The wind tunnel campaign provides a comprehensive experimental database including propellers loads measurements and velocity fields. DUST mid-fidelity solver was used to numerically reproduce some of the most interesting configurations tested in the wind tunnel, with the aim to enhance the discussion and physical comprehension of the interactional phenomena providing detrimental effects on rear propeller performance during each phase of the transition manoeuvre.

The first phase of the manoeuvre, characterised by lowest free-stream velocity and high propeller tilting angle of attack shows a substantially absent propeller-propeller interaction, thus rear propeller performance showed negligible losses in terms of thrust and power with respect to single propeller configuration. In this flight conditions, advance ratio represents an important parameter, as increasing free-stream velocity interactional phenomena arise and detrimental effects on rear propeller occur. On the other hand, the increase of vertical separation between propellers highlights beneficial effects showing an increasing recovery of single propeller performance. The last phase of transition, characterised by high advance ratios and low propellers tilting angles, shows for tandem coaxial configuration the worst configuration in terms of performance losses. Indeed, the rear propeller is almost completely invested by front slipstream that produces a reduction of blades effective angle of attack on the advancing side of the disk. An increase in the vertical separation produces a mitigation of detrimental effects on rear propeller performance. The intermediate phase of the manoeuvre is characterised by the combination of interference phenomena identified in the first and last phase of transition. Generally speaking, an increase of the propeller angle of attack provides the front slipstream to shift away from the rear propeller, thus producing slightly lower detrimental effects.

In conclusion, the comprehensive experimental data base produced during this wind tunnel campaign over a free propeller geometry repre-

sent a quite novel and suitable tool to guide the design of tilting wing eVTOL vehicles as well as to validate numerical tool with different level of fidelity. Moreover, the present work confirms the robustness of the mid-fidelity numerical solver DUST also for the investigation of such a challenging flight condition as the transition manoeuvre of a multi-rotor configuration characterised by high interactional mechanisms.

CRediT authorship contribution statement

Alex Zanotti: Writing – original draft, Validation, Supervision, Software, Project administration, Methodology, Investigation, Funding acquisition, Formal analysis, Data curation, Conceptualization. **Alessandro Velo:** Writing – original draft, Validation, Software, Methodology, Investigation, Formal analysis, Data curation. **Chiara Pepe:** Writing – original draft, Validation, Software, Methodology, Investigation, Formal analysis, Data curation. **Alberto Savino:** Writing – original draft, Supervision, Software, Methodology, Investigation, Formal analysis, Data curation, Conceptualization. **Donato Grassi:** Methodology, Investigation, Formal analysis, Data curation, Conceptualization. **Luca Riccobene:** Methodology, Investigation, Formal analysis, Data curation, Conceptualization.

Declaration of competing interest

The authors declare that they have no known competing financial interests or personal relationships that could have appeared to influence the work reported in this paper.

Data availability

Data will be made available on request.

Acknowledgements

This research was performed by using staff and facilities of Aerodynamics Laboratory of Department of Aerospace Science and Technology of Politecnico di Milano. Model manufacturing was funded by basic research funding of Politecnico di Milano.

References

[1] C. Silva, W.R. Johnson, E. Solis, M.D. Patterson, K.R. Antcliff, Vtol urban air mobility concept vehicles for technology development, in: 2018 Aviation Technology, Integration, and Operations Conference, 2018, p. 3847.
[2] H.D. Kim, A.T. Perry, P.J. Ansell, A review of distributed electric propulsion concepts for air vehicle technology, in: 2018 AIAA/IEEE Electric Aircraft Technologies Symposium (EATS), IEEE, 2018, pp. 1–21.
[3] M. Ramasamy, Measurements comparing hover performance of single, coaxial, tandem, and tilt-rotor configurations, in: AHS 69th Annual Forum, vol. 31, 2013, p. 32.
[4] D. Shukla, N. Komerath, Multirotor drone aerodynamic interaction investigation, Drones 2 (4) (2018) 43.
[5] R. de Vries, N. van Arnhem, T. Sinnige, R. Vos, L.L. Veldhuis, Aerodynamic interaction between propellers of a distributed-propulsion system in forward flight, Aerosp. Sci. Technol. 118 (2021) 107009.
[6] T.C. Stokkermans, D. Usai, T. Sinnige, L.L. Veldhuis, Aerodynamic interaction effects between propellers in typical evtol vehicle configurations, J. Aircr. 58 (4) (2021) 815–833.
[7] A. Zanotti, D. Algarotti, Aerodynamic interaction between tandem overlapping propellers in evtol airplane mode flight condition, Aerosp. Sci. Technol. 124 (2022) 107518.
[8] R. Piccinini, M. Tugnoli, A. Zanotti, Numerical investigation of the rotor-rotor aerodynamic interaction for evtol aircraft configurations, Energies 13 (22) (2020) 5995.
[9] G. Droandi, G. Gibertini, D. Grassi, G. Campanardi, C. Liprino, Proprotor–wing aerodynamic interaction in the first stages of conversion from helicopter to aeroplane mode, Aerosp. Sci. Technol. 58 (2016) 116–133.
[10] C. Sheng, J.C. Narramore, Computational simulation and analysis of bell boeing quad tiltrotor aero interaction, J. Am. Helicopter Soc. 54 (4) (2009) 42002.
[11] Airbus, Vahana project, 2019–2020, https://acubed.airbus.com/projects/vahana.
[12] M. Tugnoli, D. Montagnani, M. Syal, G. Droandi, A. Zanotti, Mid-fidelity approach to aerodynamic simulations of unconventional vtol aircraft configurations, Aerosp. Sci. Technol. 115 (2021) 106804.
[13] D. Algarotti, Experimental-numerical investigation of the aerodynamic interaction between tandem propellers in evtol airplane mode, 2021.
[14] A. Zanotti, D. Algarotti, Aerodynamic interaction between tandem overlapping propellers in evtol airplane mode flight condition, Aerosp. Sci. Technol. 124 (2022) 107518, https://doi.org/10.1016/j.ast.2022.107518, https://www.sciencedirect.com/science/article/pii/S1270963822001924.
[15] W. Zhou, Z. Ning, H. Li, H. Hu, An experimental investigation on rotor-to-rotor interactions of small uav propellers, in: Proceedings of the 35th AIAA Applied Aerodynamics Conference, Denver, USA, 2017.
[16] T. Stokkermans, D. Usai, T. Sinnige, V. LLM, Aerodynamic interaction effects between propellers in typical evtol vehicle configurations, J. Aircr. 58 (4) (2021) 815–833, https://doi.org/10.2514/1.C035814.
[17] J. Hackett, P. Ashill, M. Mokry, Wall correction methods for powered models of conventional take off and landing aircraft, in: Wind Tunnel Wall Corrections, AGARD AG-336, 1998, p. 7.
[18] T.C. Stokkermans, L.L. Veldhuis, Propeller performance at large angle of attack applicable to compound helicopters, AIAA J. 59 (6) (2021) 2183–2199.
[19] M. Raffel, C. Willert, S. Wereley, J. Kompenhans, Particle Image Velocimetry — a Practical Guide, Springer, Berlin, 2007.
[20] N. Polaczyk, E. Trombino, P. Wei, M. Mitici, A review of current technology and research in urban on-demand air mobility applications, in: Proceedings of the Vertical Flight Society's 6th Annual Electric VTOL Symposium, Mesa, AZ, USA, 2019.
[21] G. Droandi, M. Syal, G. Bower, Analysis of the interactional aerodynamics of the vahana evtol using a medium fidelity open source tool, in: Proceedings of the VFS Aeromechanics for Advanced Vertical Flight Technical Meeting, AHS International, San Jose, CA, USA, 2020.
[22] G.-H. Cottet, P.D. Koumoutsakos, D. Petros, et al., Vortex Methods: Theory and Practice, Cambridge University Press, 2000.
[23] G.S. Winckelmans, Topics in vortex methods for the computation of three-and two-dimensional incompressible unsteady flows, Ph.D. thesis, California Institute of Technology, 1989.
[24] D. Montagnani, M. Tugnoli, F. Fonte, A. Zanotti, G. Droandi, M. Syal, Mid-fidelity analysis of unsteady interactional aerodynamics of complex vtol configurations, in: 45^{th} European Rotorcraft Forum, Warsaw, Poland, Sept. 2019, 2019.
[25] S. Gallay, E. Laurendeau, Nonlinear generalized lifting-line coupling algorithms for pre/poststall flows, AIAA J. 53 (7) (2015) 1784–1792.
[26] M. Drela, Xfoil: an analysis and design system for low Reynolds number airfoils, in: T.J. Mueller (Ed.), Low Reynolds Number Aerodynamics, Springer Berlin Heidelberg, Berlin, Heidelberg, 1989, pp. 1–12.
[27] L.A. Viterna, D.C. Janetzke, Theoretical and experimental power from large horizontal-axis wind turbines, Tech. Rep., NASA Lewis Research Center, Cleveland, OH (United States), 1982.
[28] C. Pepe, A. Velo, Experimental and numerical investigation of aerodynamic interaction between tandem propellers in conversion manoeuvre, Master's thesis, Politecnico di Milano, 2023.
[29] B. Ortun, R. Boisard, I. Gonzalez-Martino, In-plane airloads of a propeller with inflow angle: prediction vs. experiment, in: 30th AIAA Applied Aerodynamics Conference, 2012, p. 2778.